Al K-edge XANES spectra of aluminosilicate minerals

DIEN LI, G. M. BANCROFT

Department of Chemistry, University of Western Ontario, London, Ontario N6A 5B7, Canada

M. E. FLEET

Department of Earth Sciences, University of Western Ontario, London, Ontario N6A 5B7, Canada

X. H. FENG

Canadian Synchrotron Radiation Facility, Synchrotron Radiation Center, University of Wisconsin, Stoughton, Wisconsin 53589, U.S.A.

Y. PAN

Department of Geological Sciences, University of Saskatchewan, Saskatoon, Saskatchewan S7N 0W0, Canada

ABSTRACT

Al K-edge X-ray absorption near-edge structure (XANES) spectra of a range of aluminosilicate and aluminum oxide minerals were collected using synchrotron radiation. The Al K-edge spectra of aluminosilicates containing fourfold-coordinated Al ([4]Al) and sixfold-coordinated Al ([6]Al) are qualitatively interpreted on the basis of a comparison with the Si K-edge spectra of α quartz and stishovite and MO calculations for tetrahedral and octahedral clusters. Some near-edge features are attributed to the multiple scattering (MS) effect from the more distant shell atoms. The Al K-edge (peak C) shifts toward higher energy with an increase in the coordination number (CN) of Al, from 1566.7 eV for [4]Al (averaged for eight samples) to 1567.8 eV for [5]Al and to 1568.3 eV for [6]Al (averaged for 17 samples). For [4]Al and [6]Al aluminosilicates, respectively, the Al K-edge shifts to higher energy with increase in the Al-O bond distance (d_{Al-O}), distortion of the Al polyhedron (Δ_{Al-O}), and decrease in the Al-O bond valence (s_{Al-O}). Also for [4]Al and [6]Al aluminosilicates, the relative intensity of the Al K-edge is correlated with the content (in weight percent) of Al in tetrahedral and octahedral sites, respectively. This correlation therefore establishes Al K-edge spectroscopy as a potential technique for semiquantitatively determining the distribution of Al between fourfold- and sixfold-coordinated sites.

INTRODUCTION

The structural coordination of Al in crystalline aluminosilicate minerals has been studied by X-ray crystallography (Smyth and Bish, 1988), X-ray emission spectroscopy (XES) (Suzuki et al., 1983), X-ray photoelectron spectroscopy (XPS) (West and Castle, 1982; Wagner et al., 1983), magic-angle-spinning nuclear magnetic resonance (MAS-NMR) spectroscopy (Sanz and Serratosa, 1984; Kinsey et al., 1985; Kirkpatrick et al., 1985; Lippmaa et al., 1986; Kirkpatrick, 1988), and Al K-edge X-ray absorption spectroscopy (XAS) (Brytov et al., 1979; Brown et al., 1983; McKeown et al., 1985; McKeown, 1989). Al in aluminosilicates is normally fourfold or sixfold coordinated with O, but Al is also known to be fivefold coordinated in andalusite ([6]Al[5]AlSiO5) (Winter and Ghose, 1979; Cruickshank et al., 1986; Alemany and Kirker, 1986; Alemany et al., 1991; Dec et al., 1991). Therefore, Al should act as both a network former ([4]Al) and a network modifier ([6]Al) in aluminosilicate glasses and melts.

In this paper, we report Al K-edge X-ray absorption near-edge structure (XANES) spectra of a range of crystalline aluminosilicate minerals. Our purposes are the following: (1) to interpret the Al K-edge spectra based on MO calculations and comparison of Al K-edge spectra with the Si K-edge spectra of [4]Si in α quartz and [6]Si in stishovite; (2) to explore qualitative correlations of the shift in the Al K-edge with the coordination number (CN) of Al, Al-O bond distance (d_{Al-O}), Al-O bond valence (s_{Al-O}), and distortion of the coordination polyhedra (Δ_{Al-O}), as well as chemical composition of the first and second neighbor shells; and (3) to document a semiquantitative relationship between the intensity of the Al K-edge and the content of Al in both octahedral and tetrahedral sites and to investigate the partitioning of Al between tetrahedral and octahedral sites. This work establishes a foundation for the use of the Al K-edge XANES method in the study of the structural role of Al in glasses and melts.

EXPERIMENTAL METHODS

Aluminosilicate mineral samples were largely obtained from the Department of Earth Sciences, University of Western Ontario. The samples were characterized by optical petrography and powder X-ray diffraction (PXRD)

TABLE 1. Electron microprobe analyses (in weight percent) of aluminosilicate minerals

Mineral	SiO₂	Al₂O₃	MgO	CaO	Na₂O	K₂O	FeO	MnO	TiO₂	Cr₂O₃	Cl	F	Total
Anorthite	44.25	34.83		19.38	0.55		0.56						99.52
Microcline	65.00	18.22			0.61	16.04	0.03						99.89
Sodalite	37.07	31.46		0.01	24.49	0.03					7.21		100.30
Biotite*	38.00	10.31	13.30		0.54	8.95	17.89	0.90	2.07		0.19	2.57	94.74
Cordierite	49.65	33.24	9.50		0.33		5.44	0.07					98.21
Spodumene**	64.35	26.70			0.05			0.06					91.23
Pyrope	42.30	21.92	18.58	5.31			8.66	0.44	0.09	2.22			99.51
Almandine	39.34	22.06	10.54	5.11			21.84	0.49	0.11				99.50
Spessartine	36.39	20.12	0.09	3.74			8.07	31.55	0.12				100.10
Grossular	39.06	22.89		35.35	0.03		1.52	0.59	0.12				98.52
Clinozoisite†	37.92	26.08	0.01	23.51			8.93	0.07	0.19	0.01			96.72
Epidote†	37.01	23.13	0.06	23.01	0.01		13.63	0.20	0.19				97.23
Kyanite	37.03	62.21	0.01				0.17	0.04					99.46
Topaz	31.79	55.78										12.33	99.65
Beryl**	62.77	16.87			0.92				0.01				80.57
Tourmaline**	38.10	40.41		0.89	1.59		0.01	0.29				0.64	81.93
Corundum		99.48					0.37			0.27			100.10
Muscovite*	45.13	33.10	0.83	0.03	0.57	10.25	2.73		0.39			0.85	93.88
Omphacite	57.24	13.18	7.51	12.09	7.53		2.12	0.04	0.08	0.02			99.82
Sillimanite	37.19	62.46					0.29						99.94
Andalusite	37.26	62.65					0.23						100.10

* H₂O in this mineral was not determined.
** Li in spodumene, Be in beryl, and B in tourmaline were not determined.
† Fe in this mineral is Fe₂O₃ rather than FeO.

at the University of Western Ontario, and by electron microprobe analysis (EMPA) at the University of Saskatchewan. The EMPA results are summarized in Table 1. The sodalite sample was a mixture of sodalite and K-rich nepheline. The sillimanite was fibrolitic and apparently a mixture including other aluminosilicates and hydrous alteration phases. All other minerals were single phase, departing from ideal end-member compositions only because of expected solid solutions.

Al K-edge XANES spectra of the aluminosilicate minerals were collected on the Double Crystal Monochromator (DCM) beamline (Yang et al., 1992), Canadian Synchrotron Radiation Facility (CSRF), which is accommodated in the Synchrotron Radiation Center (SRC), University of Wisconsin. Two α-quartz crystals, cut along the orientation (10$\bar{1}$0) (2d = 8.512 Å), were employed as monochromators, with a resolution of about 0.7 eV. However, the intensity of the photon flux at the Al K-edge energy range was very weak; <1% of that from the InSb (111) monochromator for the Si K-edge measurement (Li et al., 1993, 1994). The spectra were taken at room temperature and a chamber pressure of about 10^{-7} torr using the Aladdin synchrotron radiation source operating at 800 MeV or 1 GeV.

The aluminosilicate minerals were ground into fine powder of about 10 μm particle size, and the powder samples were pressed uniformly on electric C tape supported on a stainless steel sample holder for XANES measurements. The Al K-edge spectra were recorded over the energy ranges 1565–1572 eV (0.1 eV for each data point) and 1572–1600 eV (0.25 eV for each data point) using total electron yield (TEY). TEY was measured using the sample current. The spectra were normalized by I/I_0, where I is the intensity of TEY, and I_0 is the intensity of photon flux. The signal-to-noise ratios for some

spectra were poor owing to the low photon flux from the α quartz (10$\bar{1}$0) monochromator crystals. The Al K-edge spectra shown in Figures 1 and 2 are averages of five scans and have been smoothed by summing two adjacent data points. The spectra were calibrated with the Al metal edge at 1560.0 eV, and a similar linear preedge background was removed for each spectrum. The Si K-edge spectra of the aluminosilicate minerals investigated were collected separately using the InSb (111) monochromator in the DCM beamline and following the procedures of Li et al. (1993).

RESULTS AND DISCUSSION

Al K-edge XANES spectra of [4]Al

Figure 1 compares the Al K-edge XANES spectra (solid dot lines) of anorthite, microcline, and biotite with the Si K-edge spectra (solid line) of these minerals and α quartz. The Al K-edge spectra of the other aluminosilicate minerals containing [4]Al, such as sodalite, cancrinite, and cordierite, are very similar to those of anorthite, microcline, and biotite. The peak positions, measured at the peak maximum, for these aluminosilicate minerals containing [4]Al and α quartz are given in Table 2. The reading error for the edge peak C is ±0.1 eV. To enable comparison of the spectra, the Al and Si K-edge XANES spectra are aligned by setting peak C to zero on the energy scale. The intensity of peak C increases in the sequence of biotite, microcline, and anorthite. The ΔE value in Table 2 is the energy difference between each peak and peak C.

The Al K-edge spectra of these [4]Al minerals are qualitatively very similar and correspond closely to the previously published Al K-edge spectrum of albite (Brown et al., 1983; McKeown et al., 1985). Peaks C, D, E, and G lie at similar ΔE values for all the six minerals. Peak
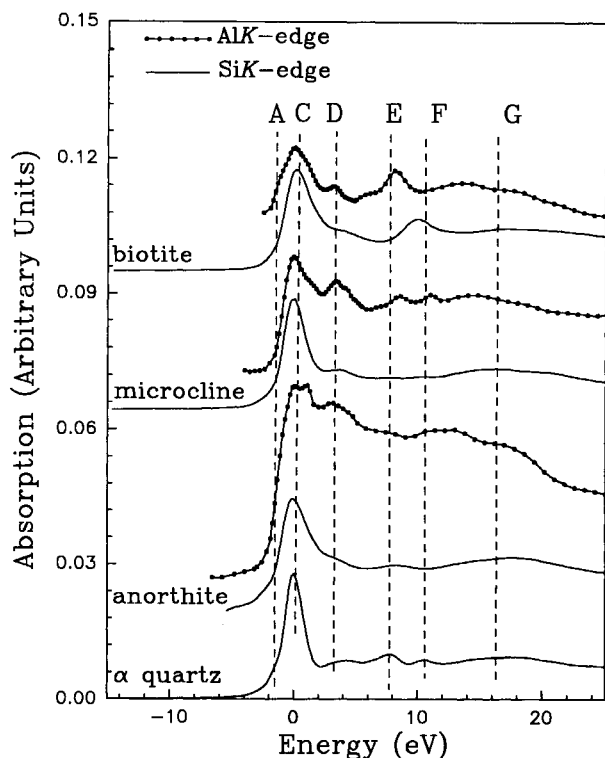
Fig. 1. Al K-edge XANES spectra of some representative [4]Al aluminosilicate minerals, namely anorthite, biotite, and microcline (solid dot lines), are compared with Si K-edge spectra of these minerals and α quartz (solid lines: Li et al., 1993). The Al and Si K-edge spectra are aligned by calibrating peak C to zero in energy scale. The spectra were collected by total electron yield (TEY); peaks A to G are features identified in Li et al. (1993, 1994) and Table 2.
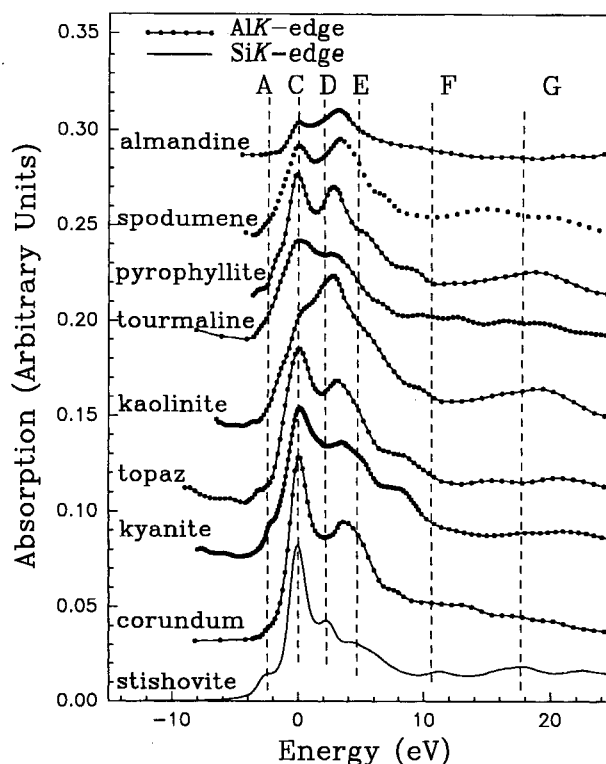
Fig. 2. Al K-edge XANES spectra of some representative [6]Al aluminosilicate minerals, namely almandine, spodumene, pyrophyllite, tourmaline, kaolinite, topaz, kyanite, and corundum (solid dot lines), are compared with Si K-edge spectrum of stishovite (solid lines: Li et al., 1993). The Al and Si K-edge spectra are aligned by calibrating peak C to zero in energy scale. Peaks A to G are features identified in Li et al. (1993, 1994) and Table 3.

C is at very similar energies for all six minerals, ranging from 1566.5 eV for microcline to 1567.3 eV for sodalite. The Si K-edge spectrum of α quartz exhibits peaks C, D, E, and F (Li et al., 1993, 1994). Interestingly, the Al K-edge spectra are qualitatively very similar to the Si K-edge spectra of the same mineral and similar to the Si K-edge spectrum of α quartz (see Fig. 1). The ΔE values for corresponding peaks are very similar in both Si and Al K-edge

spectra (see Table 2). The similarity of the Al and Si K-edge spectra is not surprising, perhaps because Si and Al reside in topologically similar tetrahedral sites. In addition, α quartz exhibits a distinct shoulder (peak A) on the lower energy side of peak C, which is not readily seen in the Al or Si K-edge spectra of the other minerals.

XANES spectroscopy of solids involves complicated processes that are not fully understood theoretically

TABLE 2. Peak positions and assignments of Al K-edge XANES of aluminosilicate minerals containing [4]Al

		Al K-edge												Si K-edge	
		Anorthite		Microcline		Sodalite		Cancrinite		Cordierite		Biotite		α quartz	
	Assignments	Peaks	ΔE	Peaks	ΔE	Peaks	ΔE	Peaks	ΔE	Peaks	ΔE	Peaks	ΔE	Peaks	ΔE
A	1s → a, (3s-like)													1844.9	−1.9
C	1s → t_2 (3p-like)	1566.9	0.0	1566.5	0.0	1567.3	0.0	1566.6	0.0	1567.0	0.0	1567.0	0.0	1846.8	0.0
D	MS	1569.9	3.0	1569.9	3.4	1570.5	3.2	1570.4	3.8	1570.1	3.1	1570.2	3.2	1850.7	3.9
E	1s → e (3d-like)	1574.3	7.4	1575.0	8.5	1575.6	8.3	1575.6	9.0	1572.7	5.7	1575.2	8.0	1854.5	7.7
F	MS	1579.2	12.3	1577.5	11.0	1580.4	13.1	1580.3	13.7			1580.5	13.5	1857.4	10.6
G	1s → t_2 (3d-like)	1584.1	17.2	1582.0	15.5	1584.2	16.9	1585.0	18.1	1582.3	15.3	1584.5	17.5	1864.3	17.5

Note: the ΔE is the energy difference between each peak and peak C rather than the energy difference between each peak and the 1s binding energy as in Li et al. (1993, 1994).

TABLE 3. Peak positions and assignments of Al K-edge XANES of representative aluminosilicate minerals containing [6]Al

| | Al K-edge | | | | | | | | | | | | | Si K-edge | |
| | Spodumene | | Pyrophyllite | | Kaolinite | | Kyanite | | Topaz | | Corundum | | Stishovite | |
Assignments	Peaks	ΔE	Peaks	ΔE	Peaks	ΔE	Peaks	ΔE	Peaks	ΔE	Peaks	ΔE	Peaks	ΔE
A 1s → a_{1g} (3s-like)	1565.9	-2.8	1565.4	-3.3	1564.7	-3.8	1565.7	-2.5	1565.8	-3.3	1566.0	-2.7	1846.3	-2.7
C 1s → t_{1u} (3p-like)	1568.7	0.0	1568.7	0.0	1568.5	0.0	1568.2	0.0	1569.1	0.0	1568.7	0.0	1849.0	0.0
D MS			1571.5	2.8	1571.3	2.8							1851.3	2.3
E 1s → t_{2g} (3d-like)	1572.0	3.3	1574.1	5.4	1574.2	5.7	1571.8	3.6	1572.7	3.4	1572.4	3.7	1853.4	4.4
F MS	1575.4	6.7	1577.8	9.1	1578.1	9.6	1580.3	13.7	1577.4	8.3	1576.8	7.9	1860.2	11.2
G 1s → e_g (3d-like)	1583.7	15.0	1584.6	15.9	1584.2	15.7	1585.0	16.8	1584.4	15.3	1582.2	13.5	1866.4	17.4

Note: the ΔE is the energy difference between each peak and peak C rather than the energy difference between each peak and the 1s binding energy as in Li et al. (1993, 1994).

(Bianconi et al., 1988). The accurate interpretation of XANES spectra is impossible without sophisticated theoretical calculation. This kind of calculation is often very difficult for solid state systems. However, our recent studies indicate that Si K- and L-edge XANES spectra of α quartz are qualitatively interpretable based on Xα multiple scattering MO calculation and XANES spectra of model gas phase molecules (Li et al., 1993, 1994; Sutherland et al., 1993). These assignments are in good agreement with the interpretation of the Si L-edge XANES spectra of gas phases SiH_4 (Friedrich et al., 1979), SiF_4 (Ferrett et al., 1988), and $Si(OCH_3)_4$ (Sutherland et al., 1993) and with the Si L-edge electron energy loss spectra (EELS) of some silicates (Hansen et al., 1992). Because [4]Al and [4]Si have similar structural environments in aluminosilicates and AlO_4^{5-} and SiO_4^{4-} clusters are isoelectronic, the [4]Al and [4]Si K-edge XANES spectra are expected to be similar and may be interpreted in a similar way.

Therefore, as shown in Table 2, the Al K-edge XANES spectra of aluminosilicates containing [4]Al are qualitatively interpreted by comparison with the Si K-edge spectrum of α quartz and the MO calculation of the AlO_4^{5-} cluster (Tossell, 1975a). Peak A is too weak to be observed in the Al K-edge spectra because it is the result of the dipole-forbidden 1s → a_1 (3s-like) transition. Peak C is assigned to the allowed transition of Al 1s electrons to the antibonding t_2 (3p-like) states. Peaks E and G are attributed to the transitions of the Al 1s electrons to the e and t_2 (3d-like) states, respectively, the so-called "symmetry-forbidden shape resonances" (Dehmer, 1972; Ferrett et al., 1986). Peaks D and F are attributable to multiple scattering (MS) from the more distant shell atoms (Li et al., 1993, 1994). As we indicated before (Li et al., 1994), peak G must certainly include a contribution of the MS effect from the more distant shell atoms. The splitting of peak C (see Fig. 1) in the anorthite spectrum is unexpected but may be related to the fact that Al has four nonequivalent positions in primitive anorthite.

Al K-edge XANES spectra of [6]Al

Figure 2 compares the Al K-edge XANES spectra (solid dot line) of some representative aluminosilicate minerals containing [6]Al (almandine, spodumene, pyrophyllite,

tourmaline, kaolinite, topaz, kyanite, and corundum) with the Si K-edge spectrum (solid line) of stishovite containing [6]Si. The peak positions and assignments for spodumeme, pyrophyllite, kaolinite, kyanite, topaz, corundum, and stishovite are summarized in Table 3. The Al K-edge spectra of the other aluminosilicate minerals containing [6]Al are, in general, very similar to those shown in Figure 2. Again the Al and Si K-edge XANES spectra are aligned by the calibration of peak C to zero in energy scale, and the intensity of peak C in the Al K-edge spectra increases in the sequence from the top to the bottom of this figure. The Al K-edge spectra of topaz and corundum are similar to the spectra in the work of Brown et al. (1983).

Peak A is weak but resolved in the spectra of most aluminosilicates containing [6]Al. Peak C is the main Al K-edge peak. Peak D, which is prominent in the Si K-edge spectrum of stishovite, is not apparent in the spectra of most aluminosilicates containing [6]Al. On the other hand, peak E shifts to lower energy and is more prominent in all the [6]Al K-edge spectra than in the stishovite Si K-edge spectrum, possibly because peaks D and E coalesce and overlap. The relative intensity of peaks C and E varies dramatically. Peak C is stronger than peak E for corundum, topaz, and kyanite, whereas peak E becomes more prominent than peak C for spodumene, almandine, and kaolinite.

The [6]Al in aluminosilicates has a similar structural environment to that of Si in stishovite, and the AlO_6^{9-} and SiO_6^{8-} clusters are isoelectronic. Based on comparison with the Si K-edge spectrum of stishovite and MO calculation of the AlO_6^{9-} cluster (Tossell, 1975b), the [6]Al K-edge XANES spectra are interpreted as follows. The weak peak A is assigned to the dipole-forbidden transition of Al 1s electrons to antibonding a_{1g} (s-like) states. This forbidden peak appears because the distortion of the coordination octahedra permits a mixture of Al s and p states. The intensity of peak A increases qualitatively in the order almandine, tourmaline, spodumene, epidote, corundum, pyrophyllite, kaolinite, topaz, and kyanite and is related to the local symmetry of Al. However, it is very difficult to evaluate the correlation between the intensity of peak A and the distortion of Al coordination, even on a semiquantitative basis. Peak C, of course, is assigned to the allowed transition of Al 1s electrons to the anti-
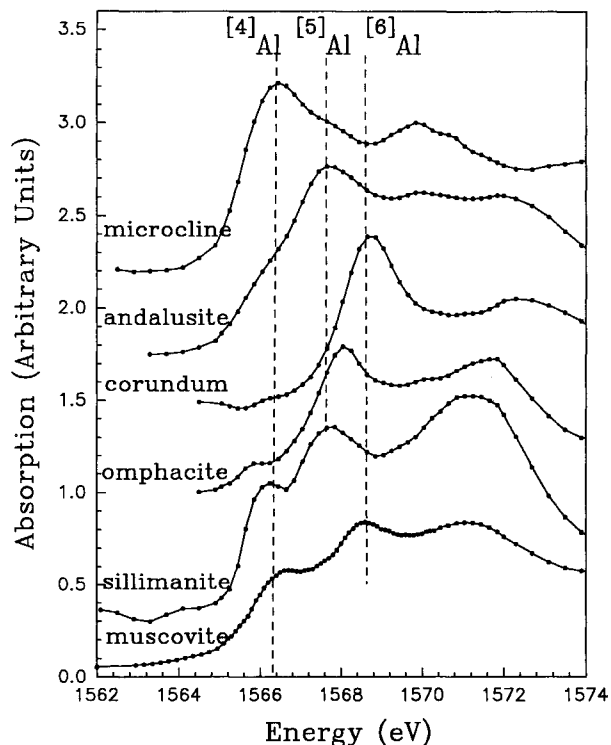
Fig. 3. Near Al K-edge spectra of microcline ([4]Al only), andalusite (both [5]Al and [6]Al), corundum ([6]Al only), and omphacite, sillimanite, and muscovite (both [4]Al and [6]Al), showing the shift of the main Al K-edge peak C to higher energy with increase in coordination number of Al.
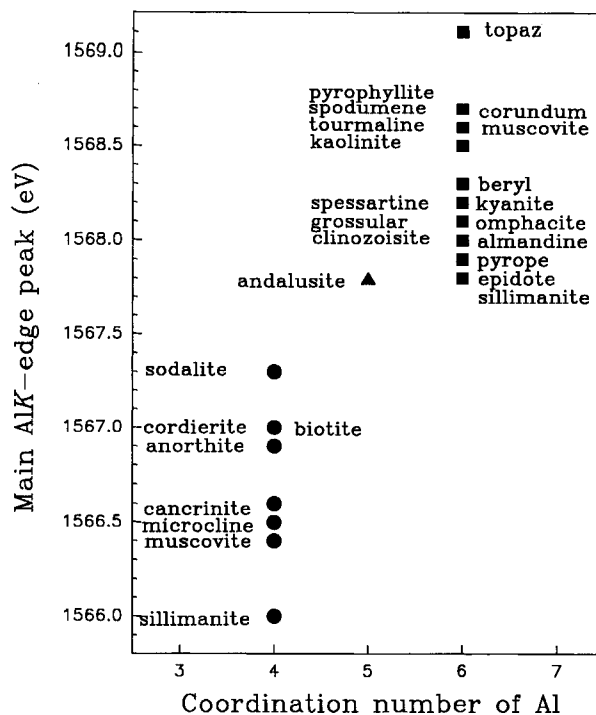

Fig. 4. Correlation of the main Al K-edge peak C of aluminosilicates with the coordination number of Al. The data used in this figure are taken from Table 4.

bonding t_{1u} (p-like) states. Peaks E and G are attributed to transitions of Al 1s electrons to t_{2g} and e_g states (d-like), respectively, or the "symmetry-forbidden shape resonance" (Dehmer, 1972; Ferrett et al., 1986). Also, as indicated above, peaks E and G certainly reflect the contribution of the MS effect from the more distant atom shells. Peak D, attributed to the MS effect in the stishovite spectrum, is resolved only in epidote, clinozoisite, beryl, and omphacite spectra and is not resolved for most aluminosilicates containing [6]Al. We suggest that it merges with peak E, making peak E appear more complicated. The MS effect enhances peak E; this interpretation is in good agreement with the MS calculation on the Al K-edge spectra (McKeown, 1989). These qualitative assignments of Al K-edge XANES of representative aluminosilicates containing [6]Al are summarized in Table 3.

Chemical shift of Al K-edge and coordination number of Al

Figure 3 compares the expanded Al K-edge spectra of microcline ([4]Al only), andalusite (both [5]Al and [6]Al), corundum ([6]Al only), and omphacite, sillimanite, and muscovite (both [4]Al and [6]Al). As stated above, the Al K-edge shifts by about 2.2 eV from 1566.5 eV for microcline to 1568.7 eV for corundum. The two major peaks

in the muscovite spectrum are at 1566.4 and 1568.6 eV. The low energy peak corresponds to [4]Al and the high energy peak to [6]Al. For andalusite, the main peak at 1657.8 eV, which is intermediate between those for [4]Al and [6]Al, is assigned to [5]Al. The edge peak for [6]Al in andalusite is not clearly resolved and probably shifts to lower energy and merges with the peak for [5]Al, and so the peak at 1567.8 eV for andalusite is very strong and broad. The shoulder at the lower energy side of the [5]Al peak is not understood, but it cannot be related to [4]Al because the sample used in this study was single-phase andalusite. The two prominent edge peaks in the sillimanite spectrum apparently indicate the presence of both [4]Al and [6]Al. However, the two peaks are consistently shifted to lower energy, and so the [6]Al edge peak is close to the [5]Al edge peak in the andalusite spectrum. Indeed, for the three polymorphs of Al_2SiO_5 (kyanite, sillimanite, and andalusite), the Al K-edge spectra cannot be interpreted completely. However, the sillimanite sample investigated was not pure, as indicated by PXRD and EMPA. Unfortunately, we were not able to re-collect the Al K-edge spectrum for sillimanite with a second sample because of the limited availability of beamline time for Al K-edge measurement.

The Al K-edge data and crystal chemical parameters, such as average Al-O bond distance (d_{Al-O} in ångströms), average Al-O bond valence (s_{Al-O}), distortion index of Al-O polyhedra (Δ_{Al-O}), coordination number (CN) of Al, rela-

TABLE 4. Al K-edge (eV) and crystal chemistry parameters of aluminosilicate minerals

Mineral	Ideal formula	Peak C (eV)	d_{Al-O} (Å)	s_{Al-O}	Δ_{Al-O}	CN	NMR δ (ppm)	Al (wt%)	I
Anorthite	Ca[Al$_2$Si$_2$O$_8$]	1566.9	1.747	3.06	1.79×10^{-4}	4		18.44	0.43
Microcline	K[AlSi$_3$O$_8$]	1566.5	1.742	3.10	2.39×10^{-6}	4	60.9	9.65	0.32
Sodalite	Na$_8$[AlSiO$_4$]$_6$Cl$_2$	1567.3	1.728	3.21		4	64.5	16.65	0.43
Cancrinite	Na$_6$Ca$_2$[AlSiO$_4$]$_6$SO$_4$(OH)$_2$	1566.6	1.742	3.10	3.28×10^{-5}	4		15.30	0.41
Biotite	K(Mg,Fe)$_3$[AlSi$_3$O$_{10}$](OH)$_2$	1567.0				4	63.5	5.45	0.17
Cordierite	Mg$_2$[Al$_4$Si$_5$O$_{18}$]	1567.0	1.750	3.05	3.47×10^{-4}	4		17.60	0.45
Pyrophyllite	Al$_2$[Si$_4$O$_{10}$](OH)$_2$	1568.7	1.912	2.97	7.65×10^{-5}	6	1.0	15.20	0.55
Kaolinite	Al$_4$[Si$_4$O$_{10}$](OH)$_8$	1568.5				6	4.0	20.30	0.64
Spodumene	LiAl[Si$_2$O$_6$]	1568.7	1.919	2.97	1.53×10^{-4}	6		14.16	0.51
Pyrope	Mg$_3$Al$_2$[Si$_3$O$_{12}$]	1567.9	1.887	3.17		6		11.60	0.23
Almandine	Fe$_3$Al$_2$[Si$_3$O$_{12}$]	1568.0	1.896	3.09		6		11.68	0.20
Spessartine	Mn$_3$Al$_2$[Si$_3$O$_{12}$]	1568.2	1.901	3.05		6		10.65	0.19
Grossular	Ca$_3$Al$_2$[Si$_3$O$_{12}$]	1568.1	1.924	2.87		6		11.88	0.28
Clinozoisite	Ca$_2$AlAl$_2$[SiO$_4$][Si$_2$O$_7$]O(OH)	1568.0	1.892	3.13	3.12×10^{-4}	6		13.81	0.19
Epidote	Ca$_2$FeAl$_2$[SiO$_4$][Si$_2$O$_7$]O(OH)	1567.8	1.895	3.11	2.70×10^{-4}	6		1.10	0.17
Kyanite	Al$_2$[SiO$_4$]O	1568.2	1.907	3.03	6.34×10^{-4}	6	7.5	32.93	0.81
Topaz	Al$_2$[SiO$_4$]F$_2$	1569.1	1.871			6		29.53	0.72
Beryl	Be$_3$Al$_2$[Si$_6$O$_{18}$]	1568.3	1.906	3.01		6	−3.2	8.93	0.30
Tourmaline	NaMg$_3$Al$_6$[Si$_6$O$_{18}$][BO$_3$]$_3$(OH)$_4$	1568.6	1.922	2.91	3.99×10^{-4}	6		21.39	0.58
Corundum	Al$_2$O$_3$	1568.7	1.913	2.99	8.72×10^{-4}	6		52.67	1.00
Muscovite	KAl$_2$[AlSi$_3$O$_{10}$](OH)$_2$	1566.4				4	67.0	5.86	0.21
		1568.6	1.940	2.79	3.87×10^{-5}	6	1.5	11.66	0.32
Omphacite	(Na,Ca)Al[(Al,Si)$_2$O$_6$]	1566.0				4			0.05
		1568.1	1.940	2.72	7.18×10^{-4}	6		6.98	0.23
Sillimanite	[4]Al[6]Al[SiO$_4$]O	1566.0	1.764	2.93	4.04×10^{-4}	4	64.5	16.30	0.28
		1567.8	1.912	2.96	3.38×10^{-4}	6	4.0	16.70	0.39
Andalusite	[5]Al[6]Al[SiO$_4$]O	1567.8	1.836	3.02	3.18×10^{-4}	5, 6	36.0	33.17	0.77

tive intensity of Al K-edge peak C, and content (in weight percent) of Al in the aluminosilicates, are compared in Table 4, together with the ^{27}Al MAS NMR peak position δ (in parts per million) (Sanz and Serratosa, 1984; Kinsey et al., 1985; Kirkpatrick et al., 1985; Lippmaa et al., 1986). The position of the Al K-edge is taken as the peak maximum of peak C in the absorption profile. Bond valence (s_{Al-O}) is calculated using the formula $s = \exp[-(R - R_0)/B]$, where R is bond length, $R_0 = 1.644$ Å, and B = 0.38 (Brown, 1985). The distortion index (Δ) is calculated using an empirical formula (Fleet, 1976),

$$\Delta = \frac{1}{N} \sum_{i=1}^{N} (R_i - R_0)^2$$

where R_i and R_0 are the individual and average radii, respectively, for a coordination polyhedron, and N is 4, 5, and 6 for [4]Al, [5]Al, and [6]Al, respectively. The relative intensity (arbitrary units) of the Al K-edge is approximately represented by the normalized height of peak C in the Al K-edge XANES spectra. The values of the relative intensity of peak C shown in Table 4 are derived using the Al K-edge spectrum of corundum as an external standard with intensity normalized to one unit. The contents (in weight percent) of Al were determined by EPMA.

Figure 4 shows the variation of the position of peak C with coordination of Al. In general, the Al K-edge shifts by about 1.6 eV with increase in coordination number of Al, from 1566.7 eV for [4]Al (averaged for eight samples) to 1568.3 eV for [6]Al (averaged for 17 samples), which is also in good agreement with the shift (2.2 eV) of the Si K-edge from α quartz to stishovite (Li et al., 1993). The Al K-edge of [5]Al is about 1567.8 eV (one sample), in-

termediate between that of [4]Al and [6]Al. The overall shift in Al K-edge toward higher energy with increase in coordination of Al is attributable to increase in the effective charge on Al atoms; qualitatively, increase in coordination number results in larger d_{Al-O} values and weaker Al-O bonding. The effective positive charge on Al atoms is higher in aluminosilicates containing [6]Al than in aluminosilicates containing [4]Al, and the [6]Al s binding energy is higher than the [4]Al s binding energy.

Figure 5 shows the correlation of Al K-edge position with ^{27}Al MAS NMR peak position (δ) for some [4]Al, [5]Al, and [6]Al aluminosilicates. The δ values are cited from Kirkpatrick et al. (1985) for anorthite, microcline, muscovite, and spodumene; Kinsey et al. (1985) for kaolinite and pyrophyllite; Lippmaa et al. (1986) for sodalite, sillimanite, andalusite, and kyanite; Sanz and Serratosa (1984) for biotite; and Sherriff et al. (1991) for beryl. The δ value for [6]Al is −3.2–7.5 ppm, whereas δ for [4]Al is 57–72 ppm, indicating that [6]Al is more shielded than [4]Al. This means that the Al-O bond for [6]Al is more ionic than that for [4]Al, parallel to the greater effective charge on [6]Al calculated from XPS and Auger energy (Nefedov et al., 1988). Therefore, the Al K-edge shifts to higher energy with increase in coordination of Al, parallel to more negative values of the ^{27}Al MAS NMR δ and increase in the effective charge on Al atoms.

Shift in Al K-edge vs. d_{Al-O}, s_{Al-O}, Δ_{Al-O}, and chemical effect

Figure 4 and Table 4 also indicate that even for aluminosilicates of the same coordination number of Al, the position of the Al K-edge (peak C) shifts significantly. For
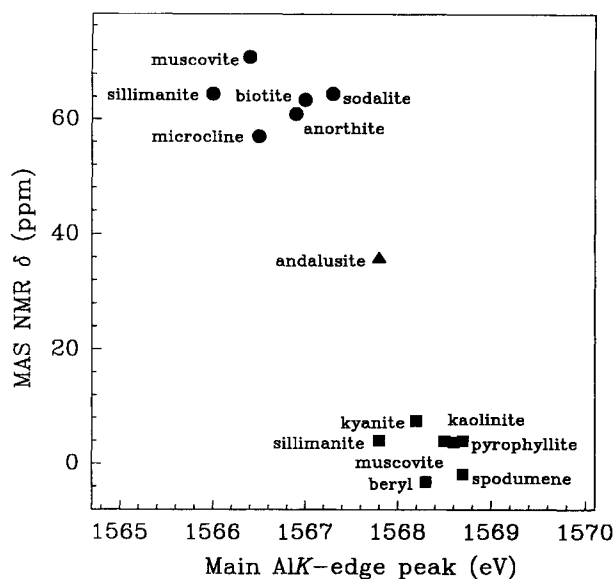
Fig. 5. Correlation of ^{27}Al MAS NMR peak position (δ) (Sanz and Serratosa, 1984; Kirkpatrick et al., 1985; Lippmaa et al., 1986) with the main Al K-edge peak of some aluminosilicates. See Table 4 and Fig. 4 for symbols.

Fig. 6. Correlations of d_{Al-O} (a), s_{Al-O} (b), and Δ_{Al-O} (c) with the main Al K-edge peak position (in electron volts). The data used in this figure are taken from Table 4 and abbreviations of mineral names follow Kretz (1983); circles are [4]Al, triangles are [5]Al, and squares are [6]Al; open symbols are data deviating from the general trends for [4]Al and [6]Al, for reasons discussed in text.

example, for aluminosilicates containing [4]Al only, the Al K-edge varies by 1.3 eV; for the aluminosilicates containing [6]Al only, it also varies by 1.3 eV. Therefore, the shift of the Al K-edge must be related to other factors, as well as coordination of Al.

Figure 6 shows correlations of d_{Al-O}, s_{Al-O}, and Δ_{Al-O} for [4]Al and [6]Al in aluminosilicates with the position of peak C in the Al K-edge spectra. The open symbols represent samples that deviate from the general trends for [4]Al and [6]Al, for reasons discussed below. For [6]Al, the dash lines have been fitted visually. The data for d_{Al-O} are from Smyth and Bish (1988) and references therein. In general, the Al K-edge shifts to higher energy with increase in d_{Al-O} and Δ_{Al-O} and with a change in coordination of Al from fourfold to sixfold, which is in agreement with the above discussion. There is a slight change in the position of peak C with s_{Al-O}. On the other hand, as seen in Figure 6, for microcline, cancrinite, anorthite, and cordierite, in which Al is fourfold coordinated, the Al K-edge shifts markedly to higher energy with increase in Δ_{Al-O} and slightly to higher energy with increase in d_{Al-O} and with decrease in s_{Al-O}. These trends are also generally observed for aluminosilicates containing [6]Al only, but the correlations are weaker. The discrepancy for omphacite, (Na,Ca)Al[(Al,Si)$_2$O$_6$], is probably related to the substitution of Fe^{2+} and Fe^{3+} for Al in the M$_1$(1) and M$_1$H sites, which leads to a larger average M-O distance (Clark and Papike, 1968). The discrepancies for topaz [Al$_2$(SiO$_4$)F$_2$] and sodalite [Na$_8$(AlSiO$_4$)$_6$Cl$_2$] are attributable to more electronegative F and Cl in the first and second neighboring shells, respectively. The shifts to lower energy of the Al K-edges for [4]Al and [6]Al in sillimanite are unexplained, but may be related to the poor quality of the sample investigated.
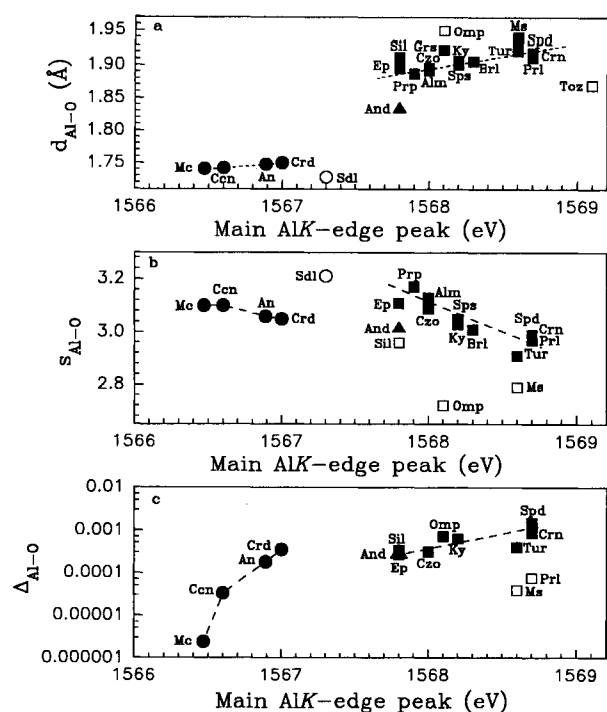
The correlations of d_{Al-O}, s_{Al-O}, and Δ_{Al-O} with the position of the Al K-edge peak C are all consistent with the dependence of Al K-edge position on effective positive charge on the absorber atom. Thus, effective positive charge should increase with increase in bond distance. Furthermore, bond distance increases with increase in polyhedral distortion, and bond valence decreases with increase in bond distance. The shifts in the position of the Al K-edge peak C at constant coordination number are not consistent with peak position being related to single or multiple scattering processes, for which increase in bond distance (R) should result in a downward shift in peak position proportional to $1/R^2$ or $1/R$ (Kasrai et al., 1991).

Intensity of Al K-edge vs. the content of Al

As noted previously, the relative intensity of peak C increases in the Al K-edge absorption spectra of Figures 1 and 2 in a downward sequence and appears to correlate with the Al content for both [4]Al and [6]Al aluminosilicate minerals (see Table 4). Figure 7 compares the relative intensity of peak C in the Al K-edge XANES spectra of aluminosilicates containing [6]Al and [4]Al with the content (in weight percent) of Al in octahedral and tetrahedral sites, respectively. The intensity of the Al K-edge has

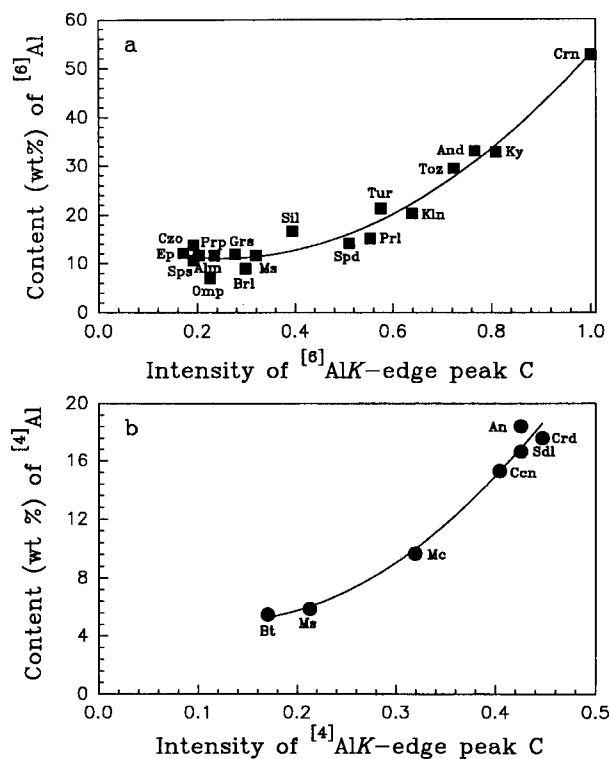Fig. 7. Correlation of the content (in weight percent) of Al for [6]Al (a) and [4]Al (b) with the intensity of the Al K-edge peak C. The intensity of the Al K-edge is simply represented by the normalized height of peak C, in arbitrary units, relative to the height of peak C in the corundum spectrum as the external standard. See Fig. 6 for abbreviations and symbols.

been estimated from the height of peak C measured by extrapolating a linear background from the preedge region and normalized to the spectrum of corundum. Peak area was not used here because we had not attempted to deconvolute the spectra. However, we are aware that peak area would more accurately reflect peak intensity, and its estimation would be required for full quantification of this technique.

For both [6]Al and [4]Al, the intensity of the Al K-edge generally increases with increase in the content of Al in the respective octahedral and tetrahedral sites. Theoretically, the absorption coefficient, μ, is proportional to the number of absorbing Al atoms, N_{Al}, and the absorption cross section. The TEY should also be proportional to N_{Al} rather than weight percent Al. Considerable care was taken to prepare finely ground and uniform samples of similar particle size and thickness, but some variation in these parameters is expected. Therefore, we did not expect the present experimental procedures and data interpretation to yield fully quantitative results. Thus, the good correlations obtained between the content (in weight percent) of [6]Al and [4]Al and intensity of Al K-edge peak C (Fig. 7) are all the more remarkable. Both correlations are not linear and are probably best fitted by equations of the

type $y = ax^2 + bx + c$, where y is the content (in weight percent) of Al and x is the normalized intensity, yielding $y = 74.34x^2 - 37.00x + 15.66$ with a correlation coefficient of 0.98 for [6]Al, and $y = 132.4x^2 - 33.39x + 7.13$ with a correlation coefficient of 0.99 for [4]Al.

These semiquantitative correlations of the content (in weight percent) of Al in respective tetrahedral and octahedral sites with the intensity of the Al K-edge peak C for [4]Al and [6]Al may be used to estimate the distribution of Al between fourfold- and sixfold-coordinated sites in aluminosilicate minerals and glasses. For example, in muscovite that contains both [4]Al and [6]Al, the contents of Al in tetrahedral and octahedral sites are 6.0 and 11.4 wt%, respectively, based on the relative intensity of the Al K-edge; these values are very close to the EMPA results. The ratio of [4]Al to [6]Al is 0.53, which is very close to the ideal value of 0.5. For omphacite, $(Na,Ca)Al$-$[(Al,Si)_2O_6]$, X-ray crystal structure refinement could not determine the distribution of Al between the tetrahedral and octahedral sites (Clark and Papike, 1968). However, the Al K-edge XANES spectrum of omphacite indicates the presence of [4]Al (see Fig. 3). The intensity ratio of [4]Al to [6]Al is about 1:5, demonstrating that for the omphacite sample presently investigated about 1.0 wt% Al substitutes for Si. This estimation for the occupancy of Al in tetrahedral sites is uncorrected for enhancement of peak C for [4]Al by overlap of peak A for [6]Al, assigned to the Al 1s → 3s transition (Table 3).

REFERENCES CITED

Alemany, L.B., and Kirker, G.W. (1986) First observation of 5-coordinate aluminum by MAS 27Al NMR in well-characterized solids. Journal of American Chemical Society, 108, 6158–6162.

Alemany, L.B., Massiot, D., Sherriff, B.L., Smith, M.E., and Taulelle, F. (1991) Observation and accurate quantification of 27Al MAS NMR spectra of some Al2SiO5 polymorphs containing sites with large quadruple interaction. Chemical Physics Letters, 17, 301–306.

Bianconi, A., Garcia, J., and Benfatto, M. (1988) XANES in condensed systems. Topics in Current Chemistry, 145, 29–67.

Brown, G.E., Dikman, F.D., and Waychunas, G.A. (1983) Total electron yield K-XANES and EXAFS investigation of aluminum in amorphous and crystalline aluminosilicates. SSRL report no. 1983/01, proposal no. 741, VII, 146–147.

Brown, I.D. (1985) The bond-valence method: An empirical approach to chemical structural bonding. In M. O'Keeffe and A. Navrotsky, Eds., Structure and bonding in crystals (2nd edition), p. 1–30. Academic, New York.

Brytov, I.A., Konashenok, K.I., and Romashchenko, Yu.N. (1979) Crystallochemical effects of AlK and SiK emission and absorption spectra for silicate and aluminosilicate minerals. Geochemistry International, 16, 142–154.

Clark, J.R., and Papike, J.J. (1968) Crystal-chemical characterization of omphacites. American Mineralogist, 53, 840–868.

Cruickshank, M.C., Dent Glasser, L.S., Barri, S.A.I., and Poplett, I.J.F. (1986) Penta-coordinated aluminum: A solid-state ^{27}Al N.M.R. study. Journal of Chemical Society, Chemical Communications, 23–24.

Dec, S.F., Fitzgerald, J.J., Frye, J.S., Shatlock, M.P., and Maciel, G.E. (1991) Observation of six-coordinate aluminum in andalusite by solid-state ^{27}Al MAS NMR. Journal of Magnetic Resonance, 93, 403–406.

Dehmer, J.L. (1972) Evidence of effective potential barriers in the X-ray absorption spectra of molecules. Journal of Chemical Physics, 56, 4496–4504.

Ferrett, T.A., Lindle, D.W., Heimann, P.A., Kerkhoff, H.G., Becker, U.E., and Shirley, D.A. (1986) Sulfur 1s core-level photoionization of SF_6. Physical Review A, 34, 1916–1930.

Ferrett, T.A., Piancastelli, M.N., Lindle, D.W., Heimann, P.A., and Shirley, D.A. (1988) Si 2p and 2s resonant excitation and photoionization in SiF_4. Physical Review A, 38, 701–710.

Fleet, M.E. (1976) Distortion parameters for coordination polyhedra. Mineralogical Magazine, 40, 531–533.

Friedrich, H., Sonntag, B., Rabe, P., Butscher, W., and Schwarz, W.H.E. (1979) Term-value and valence-Rydberg mixing in core-excite states: SiH_4 and PH_3. Chemical Physics Letters, 64, 360–366.

Hansen, P.L., Brydson, R., and McComb, D.M. (1992) p → p transitions at the silicon $L_{2,3}$-edges of silicates. Microscopy Microanalysis and Microstructure, 3, 213–219.

Kasrai, M., Fleet, M.E., Bancroft, G.M., Tan, K.H., Chen, J.M. (1991) X-ray absorption near-edge structure of alkali halides: The interatomic distance correlation. Physical Review B, 43, 1763–1772.

Kinsey, R.A., Kirkpatrick, R.J., Hower, J., Smith, K.A., and Oldfield, E. (1985) High resolution aluminum-27 and silicon-29 nuclear magnetic resonance spectroscopic study of layer silicates, including clay minerals. American Mineralogist, 70, 537–548.

Kirkpatrick, R.J. (1988) MAS NMR spectroscopy of minerals and glasses. In Mineralogical Society of America Reviews in Mineralogy, 18, 341–403.

Kirkpatrick, R.J., Kinsey, R.A., Smith, K.A., Henderson, D.M., and Oldfield, E. (1985) High resolution solid-state sodium-23, aluminum-27, and silicon-29 nuclear magnetic resonance spectroscopic reconnaissance of alkali and plagioclase feldspars. American Mineralogist, 70, 106–123.

Kretz, R. (1983) Symbols for rock-forming minerals. American Mineralogist, 68, 277–279.

Li, Dien, Bancroft, G.M., Kasrai, M., Fleet, M.E., Feng, X.H., Tan, K.H., and Yang, B.X. (1993) High-resolution SiK- and $L_{2,3}$-edge XANES of α quartz and stishovite. Solid State Communications, 87, 613–617.

Li, Dien, Bancroft, G.M., Kasrai, M., Fleet, M.E., Secco, R.A., Feng, X.H., Tan, K.H., and Yang, B.X. (1994) X-ray absorption spectroscopy of silicon dioxide (SiO_2) polymorphs: The structural characterization of opal. American Mineralogist, 79, 622–632.

Lippmaa, E., Samoson, A., and Mägi, M. (1986) High-resolution ^{27}Al NMR of aluminosilicates. Journal of American Chemical Society, 108, 1730–1735.

McKeown, D.A. (1989) Aluminum X-ray absorption near-edge spectra

of some oxide minerals: Calculation versus experimental data. Physics and Chemistry of Minerals, 16, 678–683.

McKeown, D.A., Waychunas, G.A., and Brown, G.E. (1985) EXAFS study of the coordination environment of aluminum in a series of silica-rich glasses and selected minerals within the Na_2O-Al_2O_3-SiO_2 system. Journal of Non-Crystalline Solids, 74, 349–371.

Nefedov, V.I., Yarzhemsky, V.G., Chuvaev, A.V., and Trishkina, E.M. (1988) Determination of effective atomic charge, extra-atomic relaxation and Madelung energy in chemical compounds on the basis of X-ray photoelectron and Auger transition energies. Journal of Electronic Spectroscopy and Related Phenomenon, 46, 381–404.

Sanz, J., and Serratosa, J.M. (1984) ^{29}Si and ^{27}Al high-resolution MAS-NMR spectra of phyllosilicates. Journal of American Chemical Society, 106, 4790–4793.

Sherriff, B.L., Grundy, H.G., Hartman, J.S., Hawthorne, F.C., and Cerny, P. (1991) The incorporation of alkalis in beryl: Multi-nuclear MAS NMR and crystal-structure study. Canadian Mineralogist, 29, 271–285.

Smyth, J.R., and Bish, D.L. (1988) Crystal structures and cation sites of the rock-forming minerals, 332 p., Allen and Unwin, Boston.

Sutherland, D.G.J., Kasrai, M., Bancroft, G.M., Liu, Z.F., and Tan, K.H. (1993) Si L- and K-edge X-ray-absorption near-edge spectroscopy of gas-phase $Si(CH_3)_x(OCH_3)_{4-x}$. Physical Review B, 48, 14989–15001.

Suzuki, K., Noro, H., Miyake, A., Yamamoto, Y., and Yokoi, K. (1983) Chemical effect on aluminum-potassium emission, with special reference to the melt structure of olivine-nepheline from the Kwa Nthuku cinder cone, central Kenya. Preliminary Report of African Study, 135–144.

Tossell, J.A. (1975a) The electronic structures of silicon, aluminum and magnesium in tetrahedral coordination with oxygen from SCF-X_α MO calculations. Journal of American Chemical Society, 97, 4840–4844.

———(1975b) The electronic structures of Mg, Al and Si in octahedral coordination with oxygen from SCF X_α MO calculations. Journal of Physics and Chemistry of Solids, 36, 1273–1280.

Wagner, C.D., Passoja, D.E., Hillery, H.F., Kinisky, T.G., Six, H.A., Jansen, W.T., and Taylor, J.A. (1983) Auger and photoelectron line energy relationships in aluminum-oxygen and silicon-oxygen compounds. Journal of Vacuum Science and Technology, 21, 933–944.

West, R.H., and Castle, J.E. (1982) The correlation of the Auger parameter with refractive index: An XPS study of silicates using zirconium L_α radiation. Surface and Interface Analysis, 4, 68–75.

Winter, J.K., and Ghose, S. (1979) Thermal expansion and high-temperature crystal chemistry of the Al_2SiO_5 polymorphs. American Mineralogist, 64, 573–586.

Yang, B.X., Middleton, F.H., Olsson, B.G., Bancroft, G.M., Chen, J.M., Sham, T.K., Tan, K.H., and Wallace, J.D. (1992) The design and performance of a soft X-ray double crystal monochromator beamline at Aladdin. Nuclear Instruments and Methods in Physics Research, A316, 422–436.